J Mater Sci: Mater Med (2016) 27:82
DOI 10.1007/s10856-016-5691-8

BIOMATERIALS SYNTHESIS AND CHARACTERIZATION

Original Research

A preliminary study for novel use of two Mg alloys (WE43 and Mg3Gd)

Yu Guo[1,3] · Weiwei Liu[2] · Shanshan Ma[1] · Jia Wang[1] · Jingting Zou[1] · Zhenzhen Liu[1] · Jinghui Zhao[1] · Yanmin Zhou[1]

Received: 22 October 2015 / Accepted: 21 February 2016 / Published online: 11 March 2016

Abstract In this study, two types of magnesium alloys (WE43 and Mg3Gd) were compared with Heal-All membrane (a biodegradable membrane used in guided bone regeneration) in vitro to determine whether the alloys could be used as biodegradable membranes. Degradation behavior was assessed using immersion testing with simulated body fluid (SBF). Microstructural characteristics before and after immersion were evaluated through scanning electron microscopy, and degradation products were analyzed with energy dispersive spectrometry (EDS). To evaluate the biocompatibility of the three types of materials, we performed cytotoxicity, adhesion, and mineralization tests using human osteoblast-like MG63 cells. Immersion testing results showed no significant difference in degradation rate between WE43 and Mg3Gd alloys. However, both Mg alloys corroded faster than the Heal-All membrane, with pitting corrosion as the main corrosion mode for the alloys. Degradation products mainly included P- and Ca-containing apatites on the surface of WE43 and Mg3Gd, whereas these apatites were rarely detected on the surface of the Heal-All membrane. All three type of materials exhibited good biocompatibility. In the mineralization experiment, the alkaline phosphatase (ALP) activity of 10 % Mg3Gd extract was significantly higher than the extracts of the two other materials and the negative control. This study highlighted the potential of these Mg-REE alloys for uses in bone regeneration and further studies and refinements are obviously required.

✉ Jinghui Zhao
zhaojh_1986@126.com

✉ Yanmin Zhou
2743416623@qq.com; zhouym62@126.com

[1] Department of Dental Implantology, School and Hospital of Stomatology, Ji Lin University, Changchun, People's Republic of China

[2] Department of Oral and Maxillofacial Surgery, School and Hospital of Stomatology, Ji Lin University, Changchun, People's Republic of China

[3] Jilin Provincial Key Laboratory of Tooth Development and Bone Remodeling, Changchun, People's Republic of China

1 Introduction

With the emergence and fast evolution of new medical technologies, the use of implant-supported dentures as a restoration method to treat agomphious patients has been widely accepted in recent decades. However, the quality and quantity of bone at the implant position is generally unfavorable for obtaining good osseointegration with the implants. This limitation has been addressed using guided bone regeneration (GBR), which was developed by Dahlin et al. [1–3].

To date, numerous barrier membranes have been used clinically; these membranes can be classified as resorbable or non-resorbable [4–7]. Non-resorbable membranes mainly include expanded polytetrafluoroethylene (e-PTFE) and titanium mesh [6, 7]. These membranes can provide effective barrier function and are easily managed in clinics because of their good mechanical strength and excellent biocompatibility [8]; nevertheless, secondary removal surgery was needed while using these membranes increases the pain of the patients. Commercial resorbable membranes are mainly natural or synthetic polymers and consist of collagen and aliphatic polyesters [4, 5]. Resorbable membranes do not require secondary removal surgery, but the unpredictable degradation may alter the amount of bone formation [9]. Space-making is one of the fundamental characteristics of barrier membrane, but the mechanical weakness of resorbable membranes may

impair their ability of maintaining adequate space [7] and finally lead to collapse of the barrier and a failed reconstruction [4]. Therefore, the need for alternatives to commercial resorbable products is driven by their prohibitively mechanical weakness, unpredictable degradation.

As a new class of biodegradable materials, magnesium alloys have received increased attention for orthopedic applications because of their good biocompatibility and mechanical properties [10, 11]. Magnesium may improve the formation of new bones [12], and its alloys show improved osteoconductive bioactivity [13]. However, most currently existing Mg alloys degrade rapidly, and the release of hydrogen during degradation may lead to a loss of mechanical integrity before complete bone regeneration [11, 14]. Several possible approaches used to improve the degradation rate of Mg alloys include alloying, protective coating, and surface modification [15]. Altering the content and composition of alloying elements is performed by adding rare earth elements (REEs) into Mg alloy [15–18]. The addition of REEs can improve the mechanical strength and corrosion resistance of the resulting alloys [19]. Mg–Y–Nd systems have shown good mechanical strength and corrosion resistance. Among these systems, WE43 was thought to be a suitable candidate in implant applications, especially as cardiovascular stent material [20, 21]. Gd has also been used to adjust the mechanical properties of Mg alloys for use as bio-materials with different alloy compositions [22].

In this study, Mg-REE alloys, namely, WE43 and Mg3Gd, were subjected to surface characteristic evaluation, in vitro degradation tests, and in vitro biocompatibility comparison with Heal-All membrane to assess their potential for biodegradable membranes. Moreover, Heal-All membrane, which is a resorbable membrane for clinical applications, is used as positive control.

2 Materials and methods

2.1 Preparation of magnesium alloys and Heal-All membranes

WE43 and Mg3Gd were provided by the Northwest Institute for Non-ferrous Metal Research. The alloys were extruded and shaped into a magnesium alloy sheet by using magnesium and alloying elements. Thin circular plate Mg alloy samples with dimensions of 6 mm (diameter) and 0.1 mm (thickness) were selected and ultrasonically washed with alcohol, sodium hydroxide, mixture of nitric acid and chromic acid, and alcohol for surface cleaning. Heal-All membranes (Yan Tai Zhenghai Biotechnology Corporation, Shandong, China) were prepared with the same size as the two Mg alloy samples.

2.2 Immersion test

Each specimen of WE43, Mg3Gd and Heal-All membranes was weighed (W_0) and immersed in polythene vessels containing 12 mL of simulated body fluid (SBF) solution at 37 °C for 12 days according to ISO 10993-13 and ISO 10993-15. The SBF, containing Na^+, K^+, Mg^{2+} and so forth, was prepared under the recommendation of Kokubo [23]. SBF was replenished every 48 h after recording the pH of each sample. At each immersion interval (2, 4, 6, 8, 10, and 12 d), three specimens of each type of samples were obtained; carefully washed with acetone, deionized water, 200 g/L CrO_3 combined with 10 g/L $AgNO_3$ solution, deionized water, and ethanol to eliminate degradation products; and dried naturally for about 2 h. At each considered time point, Final weight was then recorded (W_1). Corrosion rate was calculated according to Eq. (1).

$$\text{Corrosion rate (CR)} = \frac{W_0 - W_1}{A \times T} \quad (1)$$

A surface of the sample exposed to SBF solution (cm^2); T immersion time (day).

2.3 Microstructure and surface analysis

The surface morphology of each specimen was characterized by scanning electron microscopy (SEM) before immersion test. After 6 days of immersion, three specimens were gently washed with acetone, alcohol, and deionized water; dried naturally for 2 h; and subjected to SEM equipped with energy dispersive spectrometry (EDS) to evaluate microstructure and phases of the three materials. And specimens washed with 200 g/L CrO_3 and 10 g/L $AgNO_3$ solution were subjected to SEM for the evaluation of corroded surface morphology. The grains size and pits diameter were calculated using the pixel and scale bar in SEM images. Three random fields were selected to count the grains size and five random fields were selected for pits diameter.

2.4 Extract preparation

For the preparation of immersion extracts, 10 specimens of each type of samples were irradiated under UV for 30 min on each side and then immersed in Dulbecco's modified Eagle medium (DMEM) containing 10 % fetal bovine serum (FBS) with an immersion ratio of 1.25 cm^2/mL at 37 °C for 48 h, in accordance with ISO-10993. The supernatant fluid was removed, serially diluted (100, 50, and 10 %), and then refrigerated at 4 °C prior to subsequent experiments.

2.5 Cytotoxicity and cell proliferation test

Human osteoblast-like MG63 cells were cultured in DMEM containing 10 % FBS at 37 °C in humidified atmosphere with 5 % CO_2. Cytotoxicity and cell proliferation tests were performed by indirect contact. MG63 cells in the vigorous growth period were digested with trypsin to adjust the cell density to 5×10^4 or 2×10^4/mL. The cells were cultured into 96-well plates (100 μL medium/well) at 37 °C for 24 h to allow cell attachment, with 5000/well for cytotoxicity test and 2000/well for proliferation test. After the medium was removed, MG63 cells were incubated with 100 μL of diluted (10, 50, and 100 %) magnesium alloy extract, collagen membrane extract, original culture medium (negative control group), or 0.64 % phenol-containing culture medium (positive control group). Each group type has five parallel samples. The medium was replaced every 2 days. After the cells were incubated for 1, 3, and 5 days (for cytotoxicity test, cells were only incubated for 24 h), 10 μL of CCK8 (Beyotime, Shanghai, China) was added to each well. The samples were then incubated at 37 °C with 5 % CO_2 for 1 h. The plates were then shaken well, and the OD value of each well was analyzed using a microplate reader at 450 nm. Each experiment was performed in triplicate. Relative growth rate (RGR) was calculated as follows: RGR (%) = (OD value of the test group/OD value of the negative control group) × 100. According to the grading standard, RGR values were converted into five grades [24].

2.6 Cell adhesion test

Three specimens of each type of samples were initially sterilized under UV irradiation for 30 min on each side and placed into 96-well plates. MG63 cells were then seeded on the sample surfaces at a concentration of 1×10^4/sample for 6 h. Non-adherent cells were removed slightly with PBS solution. Cells were fixed with 25 % glutaraldehyde at 4 °C for 30 min, rinsed with PBS solution, and stained with 4,6-diamidino-2-phenylindole (Beyotime, Shanghai, China) at 37 °C for 20 min. Adhered cells were observed using an inverted fluorescence microscope (OLYMPUS U-RFL-T, Japan). Another three specimens incubated with MG63 for 6 h were also rinsed with PBS solution, fixed with 25 % glutaraldehyde, stored overnight at 4 °C, gradient dehydrated with ethanol, dried, coated with gold, and finally observed by SEM.

2.7 Alkaline phosphatase (ALP) assay

MG63 cells were cultured and seeded into 96-well plates for 24 h. Then the medium was discarded and 100 μL of diluted (10 and 50 %) magnesium alloy extracts or collagen membrane extracts, or original culture medium (negative control group) were added into each well of the plates. Alkaline phosphatase (ALP) activity was determined using a commercial ALP substrate kit (Nanjing Jiancheng Bioengineering Institute, Jiangsu, China). After MG63 cells were incubated for 3, 5, and 7 days, the culture medium was discarded. Cells were then gently washed twice with PBS solution and then lysed with 100 μL of 1 % Trixon-100 at 4 °C for 30 min. Cell lysates were then harvested. Another 96-well plate was added with 30 μL of the cell lysates (test group), 30 μL of 0.02 mg/mL standard phenol solution (positive control group), and 30 μL of deionized water (negative control group). The mixtures were then performed according to the manufacturer's instructions and finally, the 96-well plates was shaken slightly for 15 s, and the OD value of each well was analyzed by a microplate reader at 520 nm. The ALP assay was performed in triplicate. ALP activity was calculated according to Eq. (2).

$$\text{ALP activity} = \frac{OD_1 - OD_0}{OD_2 - OD_0} \times \frac{C_1}{C_2} \quad (2)$$

OD_1: the OD value of the test group; OD_2: the OD value of the positive group; OD_0: the OD value of the negative group; C_1: the concentration of standard phenol solution, 0.02 mg/mL; C_2: the concentration of total cellular protein.

Total protein in cell lysates was determined using a bicinchoninic acid protein assay kit (Beyotime, Shanghai, China), according to the manufacturer's instructions.

2.8 Statistical analysis

Data on weight loss and OD values were calculated and presented as mean ± standard deviations. One-way ANOVA was performed with SPSS 17.0 software to determine statistically significant differences among different groups. $P < 0.05$ was considered statistically significant.

3 Results

3.1 Microstructures before and after immersion

The microstructures of WE43 and Mg3Gd showed numerous small particles and bright intermetallic phases and obviously, more particles were observed on Mg3Gd. The grain size was from 5 to 40 μm for WE43 and from 5 to 60 μm for Mg3Gd. For Heal-All membrane, the cross-linked collagen fibers were arranged irregularly and formed a nest-like micro-appearance with no beads formed (Fig. 1c). After 6 days of immersion in SBF and acid washing, the microstructures of the materials were shown in Fig. 2. Pitting corrosion was predominant during

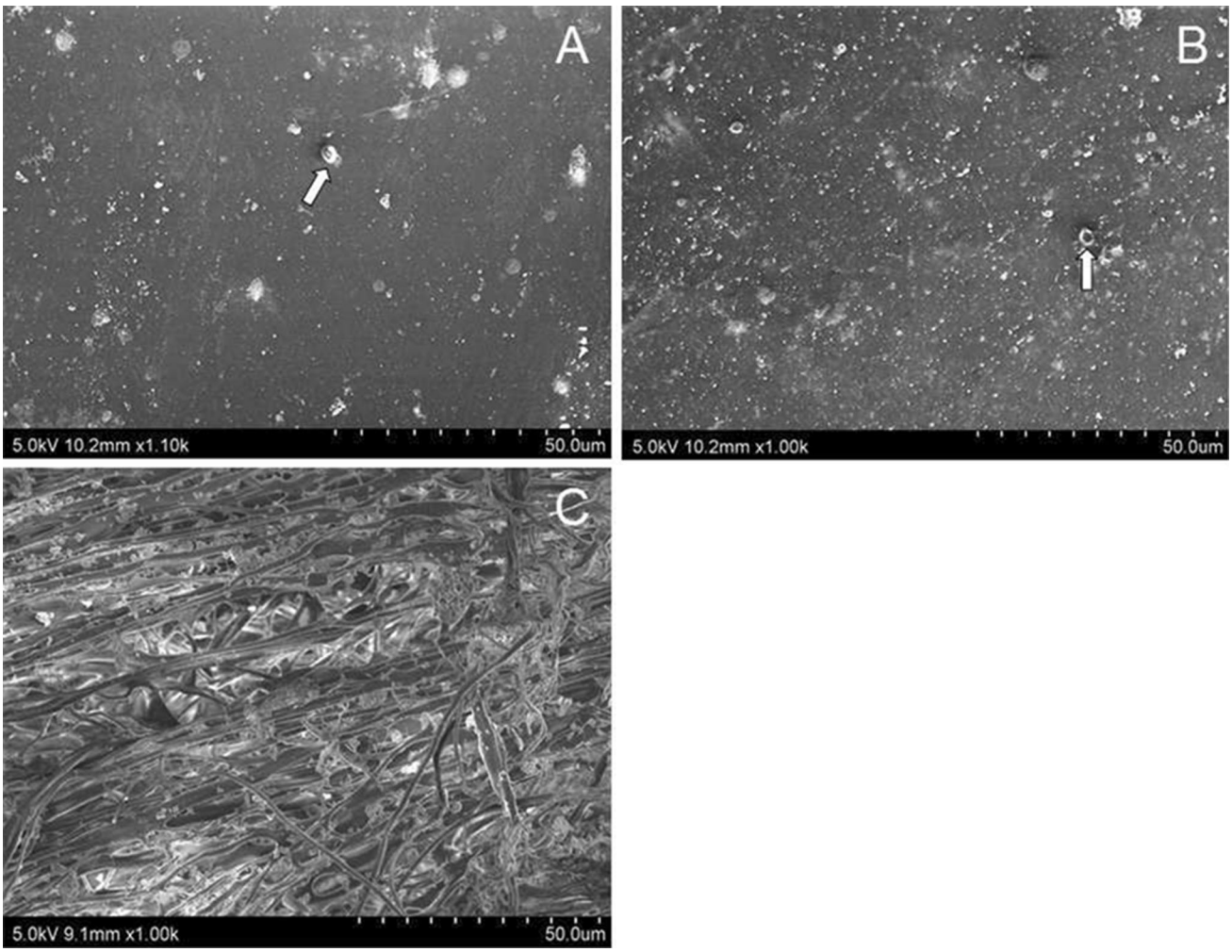

Fig. 1 SEM image of **a** WE43, **b** Mg3Gd, and **c** Heal-All membrane before immersion; the *arrow* indicates the particles on the surface

degradation for two Mg alloys, which is consistent with other studies [25] (Fig. 2a). The average diameter of pits on WE43 was 9.041 ± 3.536 μm with scale from 5 to 20 μm, while it was 8.329 ± 5.262 μm with scale from 3 to 25 μm. It seemed that the pitting corrosion of Mg3Gd was less-uniform than WE43 due to the pits diameter and the SEM images in Fig. 2a, b. However, no pores were formed though many pits could be seen on surface of Mg alloys indicated that the Mg matrix was still intact at the sixth day. As for Heal-All membrane, though some collagen fibers cracked, the nest-like micro-structure and the collagen matrix remained virtually intact after 6 days of immersion (Fig. 2c).

3.2 In vitro corrosion behavior and degradation products

To compare the degradation behavior of Mg alloys with that of the Heal-All membrane, we performed immersion testing. WE43 and Mg3Gd exhibited similar trend of the corrosion rate curve, that is, they corroded rapidly during the first 2 days. Corrosion rate decreased during the next 6 days and then remained virtually stable during the succeeding 4 days. Mg3Gd corroded faster than WE43, but the difference was not statistically significant. Meanwhile, the corrosion rate of the Heal-All membrane remained at low levels during the entire period and was lower than that of WE43 and Mg3Gd at any immersion interval, and the difference was statistically significant.

Figure 3b presents pH changes in the SBF solution. The pH of SBF containing WE43 and Mg3Gd increased with immersion time, especially during the first 2 days, which indicates that the degradation of Mg alloys can produce an alkaline micro-environment. By contrast, the degradation of Heal-All membrane produced a weakly acidic microenvironment as the pH decreased with immersion time.

The microstructures of the three materials after 6 days of immersion prior to acid washing are shown in Fig. 4.

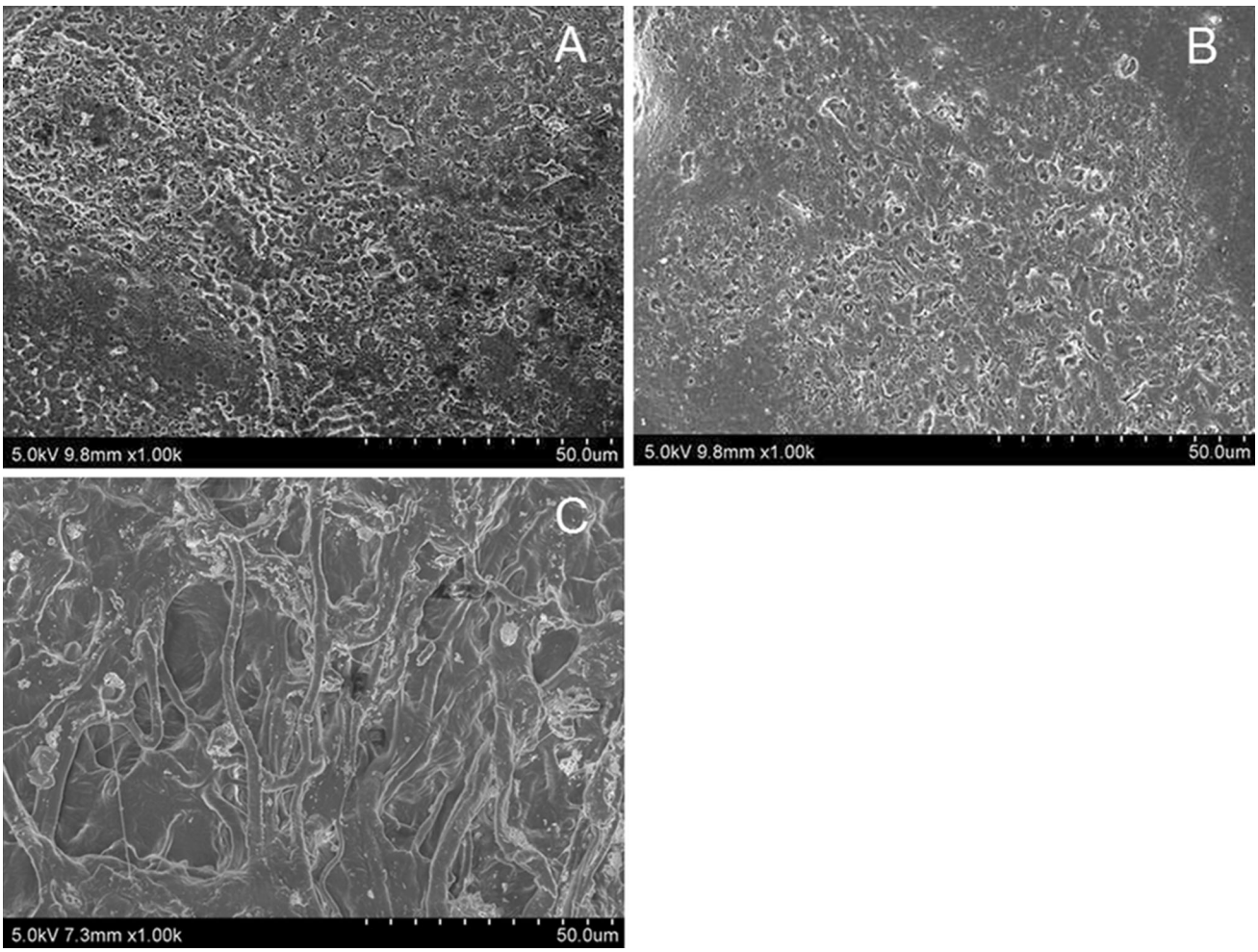

Fig. 2 SEM image of **a** WE43, **b** Mg3Gd, and **c** Heal-All membrane after immersion and acid washing

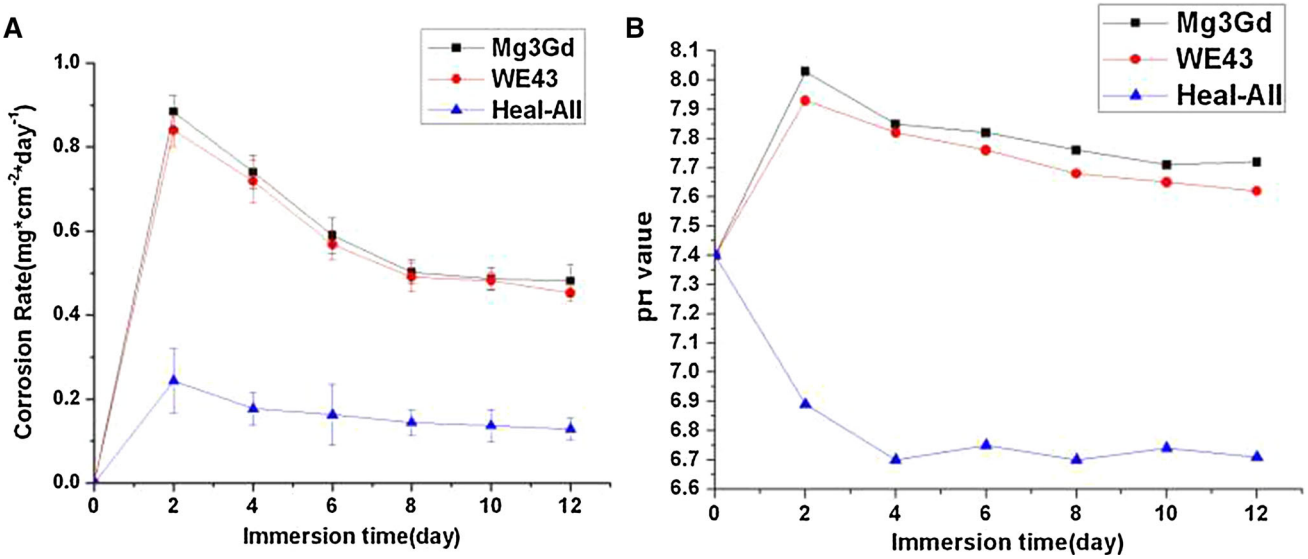

Fig. 3 **a** Corrosion rate of Mg3Gd, WE43, and Heal-All membrane in SBF, and **b** changes in pH of SBF during the immersion period

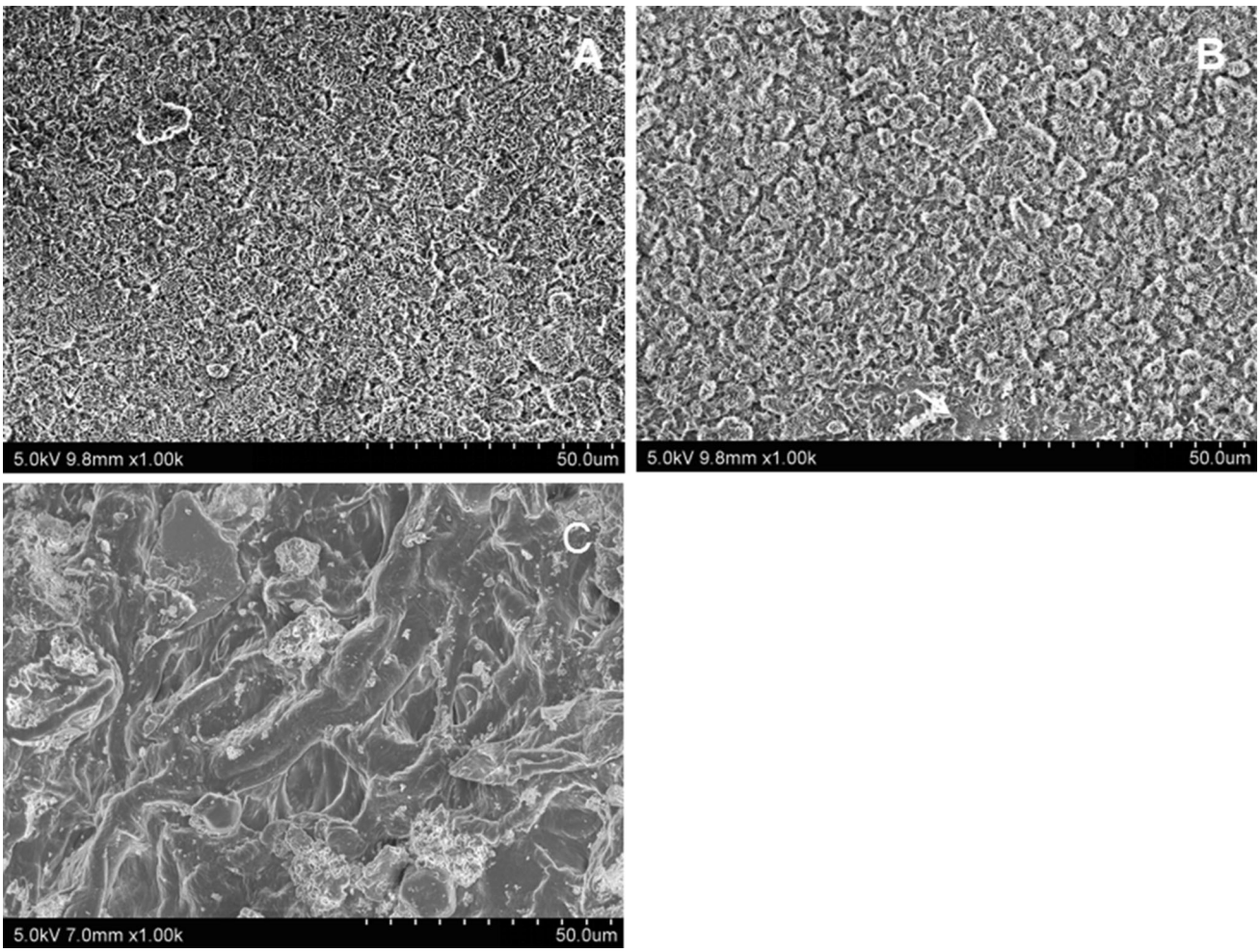

Fig. 4 SEM images of **a** WE43, **b** Mg3Gd, and **c** Heal-All membrane after immersion; the arrow shows the bare Mg matrix on the Mg3Gd surface

Salt precipitates almost completely covered the WE43 surface (Fig. 4a). While the Mg matrix was still observed on the Mg3Gd surface (Fig. 4b). And slight salt precipitation was detected on the surface and inner part of Heal-All membrane (Fig. 4c). However, whether the precipitates were formed during degradation remained unclear.

The composition of salt precipitates on the sample surface after 6 days of immersion is shown in Fig. 5 with the EDS data. Salt deposited on the sample surface included Ca- and P-containing apatites (Fig. 5a, b). As the only type of calcium phosphate crystal in calcified tissues, such as bones and teeth, calcium phosphate apatite exhibits good osteoconductivity to facilitate bone formation on the surface [26]. As shown in Fig. 5c, only a small amount of Ca- and P-containing apatites was detected on the Heal-All membrane.

3.3 In vitro biocompatibility

3.3.1 Cytotoxicity and proliferation of MG63

Cytotoxicity testing was performed with CCK-8. The relative proliferation rate (RPR) of the negative control was used as the 100 % baseline. The relationship between cell RPR and cytotoxicity grade is shown in Table 1 [24]. For WE43 and Mg3Gd, 100 % extract reduced the viability of MG63 cells, whereas 50 and 10 % extracts did not significantly reduce cell viability (Fig. 6a, b). For the Heal-All membrane, no significant reduction in viability was detected in 100, 50, and 10 % extracts (Fig. 6c). The cytotoxicity grades of all kinds of extract media were "0" or "1," except for 100 % Mg3Gd extract, whose cytotoxicity grade was "2" (Table 2).

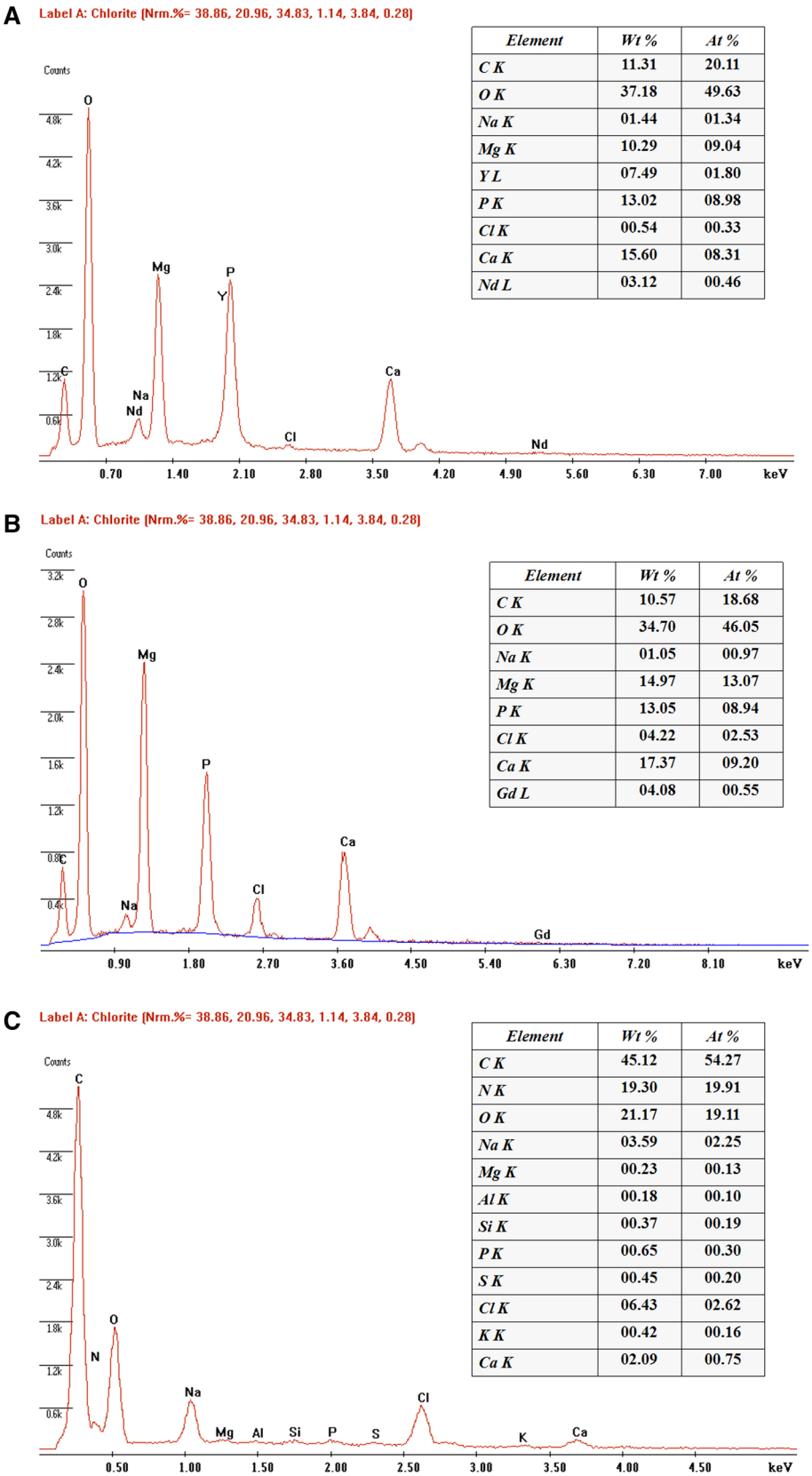

Fig. 5 EDS of **a** WE43, **b** Mg3Gd, and **c** Heal-All membrane after 6 days of immersion in SBF

Table 1 Relationship of cell RGR and cytotoxicity grade in Pharmacopoeia in the United States

RGR (%)	Cytotoxic grade
≥100	0
≥80	1
≥50	2
≥30	3
≥0	4

The proliferation test showed comparable results with cytotoxicity test results in Fig. 7. For WE43, 100 % extract significantly reduced the viability of MG63 cells during the entire period, 10 % extract increased cell viability at day 1, and 50 % extract increased cell viability at day 5 (Fig. 7a). For Mg3Gd, 100 % extract showed the most serious inhibition on MG63 cell viability during the entire period among all the experimental groups, whereas 10 % extract increased cell viability at day 5 (Fig. 7b). However, cell proliferation was not inhibited at any concentration of the Heal-All membrane extract with increasing immersion time. The 100 % extract promoted cell proliferation at days 3 and 5 (Fig. 7c).

Figure 8 shows the results of cell viability. Among 100 % extracts, that of the Heal-All membrane evidently promoted cell proliferation compared with WE43 and Mg3Gd at any time interval (Fig. 8a). For 50 % extract, cell viability at day 5 was in the order of WE43 > Heal-All > Mg3Gd (Fig. 8b). Among 10 % extracts, WE43 significantly promoted cell proliferation compared with Heal-All membrane at day 1 (Fig. 8c).

3.3.2 Cell adhesion

The results of MG63 cell adhesion test on the surface of WE43, Mg3Gd, and Heal-All membrane are shown in Figs. 9 and 10. The number of MG63 cells adhered on the surface was almost the same among the three materials. MG63 cells adhered to the surface and cracks on WE43 and Mg3Gd by their pseudopods (Fig. 10a, b). On the Heal-All membrane, MG63 cells migrated into the pores and were surrounded by collagen fibers (Fig. 10c).

3.3.3 ALP activity

ALP activity is one of the most widely used markers for early osteoblastic differentiation [27]. According to the

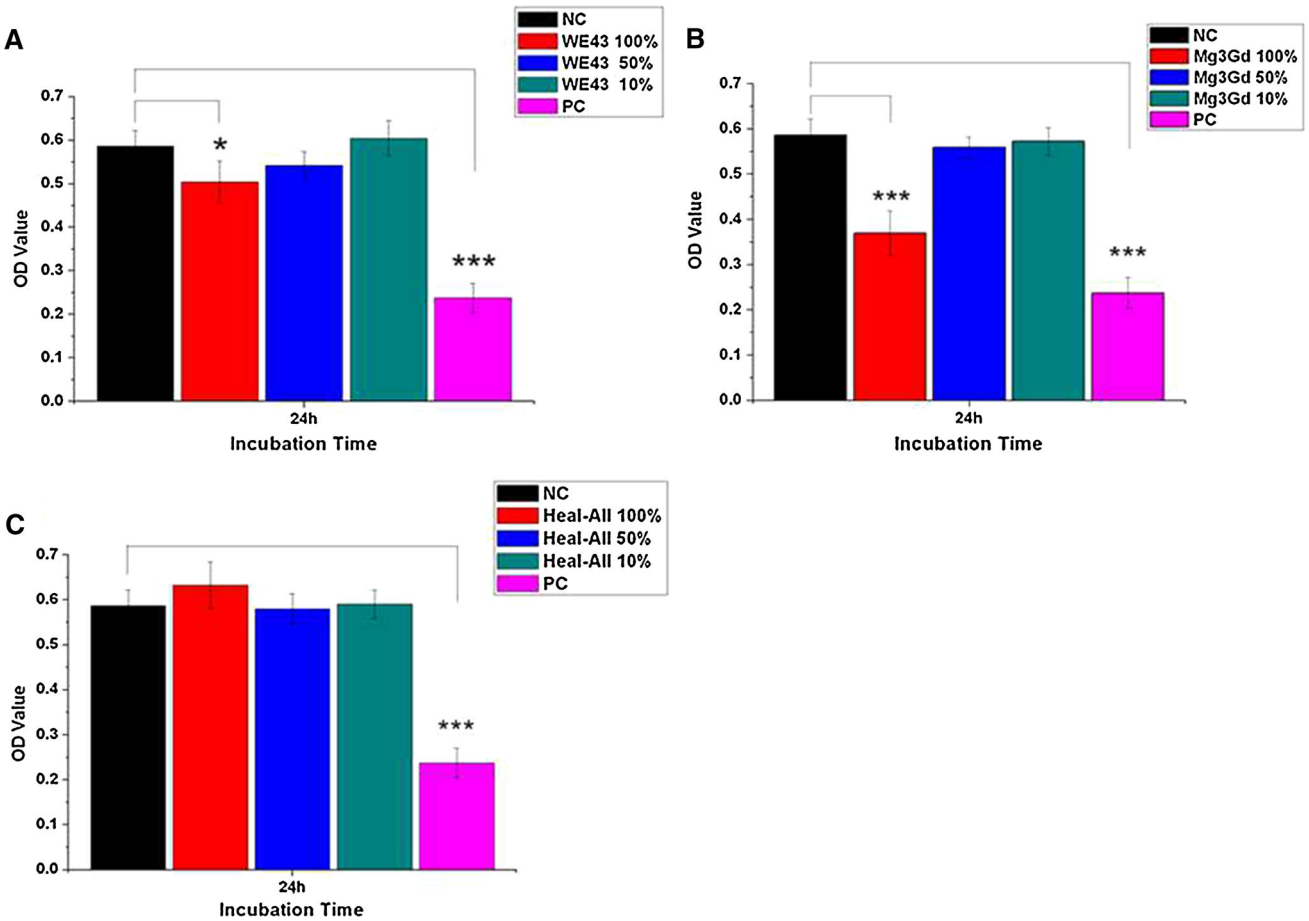

Fig. 6 Results of cytotoxicity test of **a** WE43, **b** Mg3Gd, and **c** Heal-All membrane (*$P < 0.05$, **$P < 0.01$, ***$P < 0.001$)

results of cytotoxicity and proliferation tests, 50 and 10 % extracts were selected for ALP assay. ALP activity increased for most groups with increasing immersion time (Fig. 11a, b). For 50 % extracts, ALP activity was not statistically significantly different among different groups at any time interval, except in group 50 % Mg3Gd at days 3 and 7 (Fig. 11a). By contrast, for 10 % extracts, the ALP activity of the Mg3Gd group was evidently higher than that of the other groups at days 5 and 7, and the difference was statistically significant (Fig. 11b). Thus, Mg3Gd fabricated in such shape may be more osteoconductive than WE43 and Heal-All membrane.

Table 2 Cytotoxicity after culture for 24 h

Group	RGR (%)	Cytotoxic grade
NC	100	0
WE43 100 %	86.07	1
WE43 50 %	92.46	1
WE43 10 %	103.16	0
Mg3Gd 100 %	62.99	2
Mg3Gd 50 %	95.36	1
Mg3Gd 10 %	97.59	1
Heal-All 100 %	107.80	0
Heal-All 50 %	98.92	1
Heal-All 10 %	100.57	0
PC	40.52	3

4 Discussion

Research on GBR is underway. At present, various commercial GBR membranes are available for clinical use. A barrier membrane should fulfill the following five main criteria to be used in GBR surgery: biocompatibility, space making, cell occlusiveness, tissue integration, and clinical

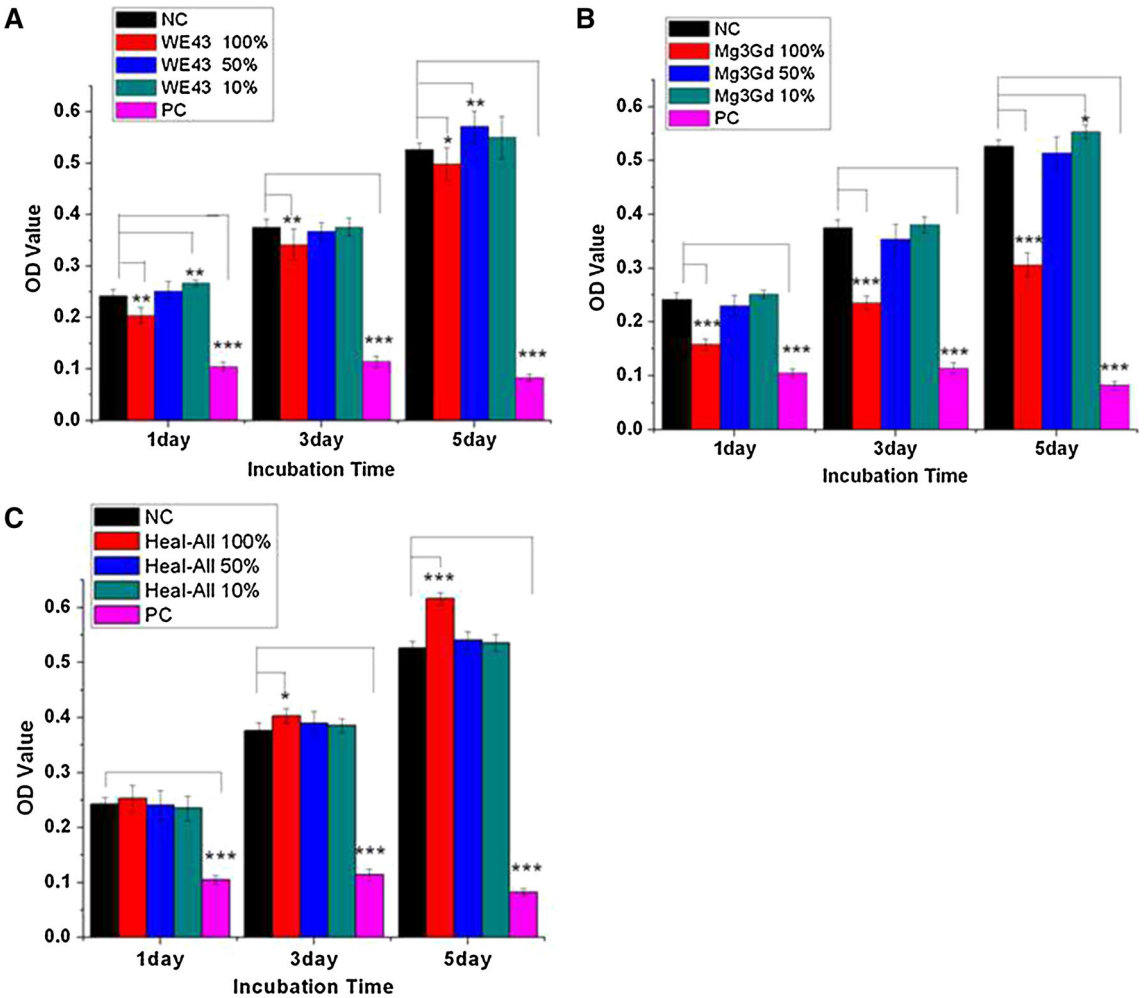

Fig. 7 Proliferation of MG63 cells cultured in **a** WE43, **b** Mg3Gd, and **c** Heal-All membrane extracts for 1, 3, and 5 days (*$P < 0.05$, **$P < 0.01$, ***$P < 0.001$)

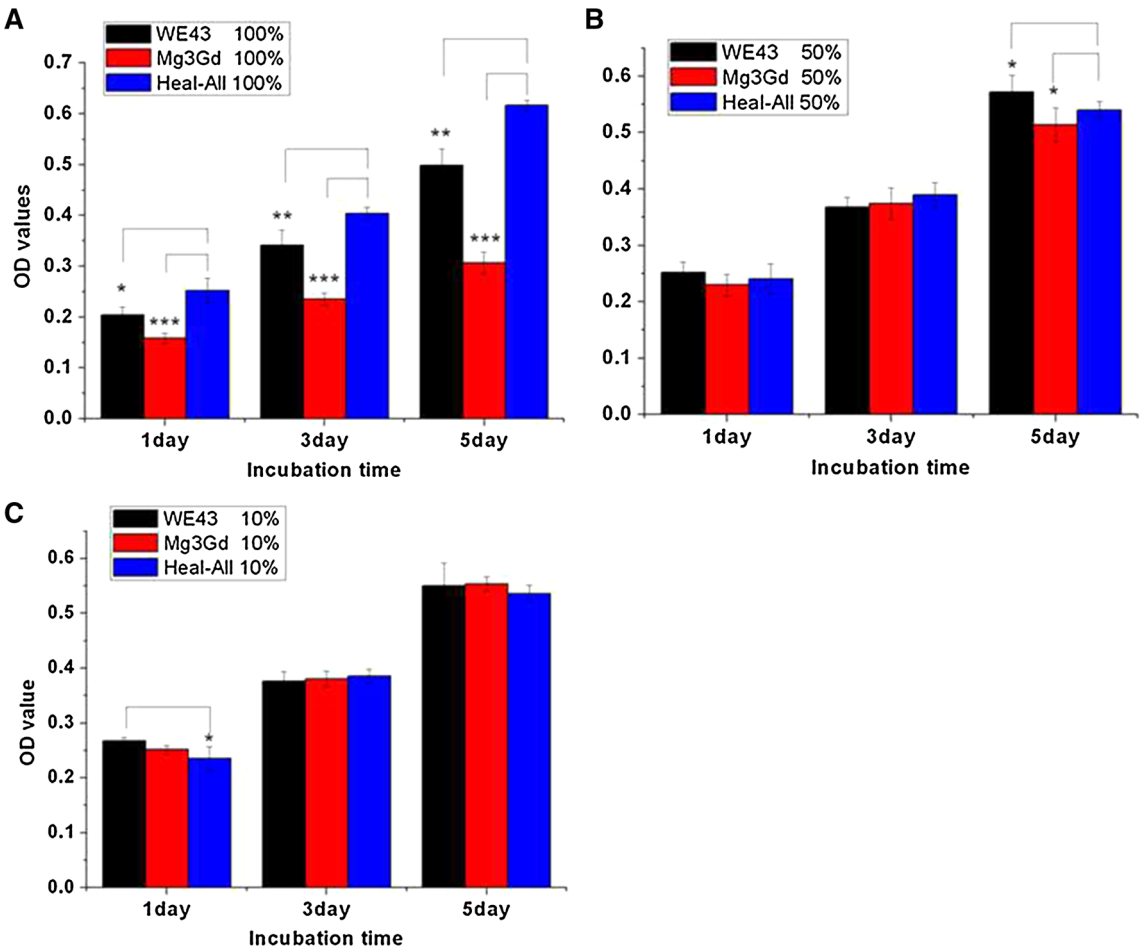

Fig. 8 Proliferation of MG63 cells cultured in **a** 100 %, **b** 50 %, and **c** 10 % extracts for 1, 3, and 5 days (*$P < 0.05$, **$P < 0.01$, ***$P < 0.001$)

manageability, as described by Scantlebury [28]. Heal-All membrane is generally used as GBR membrane for clinical applications in China made in a standardized, controlled purification process from acellular dermal matrix of cowhide. It has a bilayer structure composed of a compact and porous layer. The compact layer of the membrane possesses a smooth and condensed surface to protect against connective tissue infiltration, while the porous layer permits cellular attachment. The main composition, collagen, is supposed to degraded completely within 6 month according to manufacturer. However, long and unpredictable degradation time, mechanical weakness, and severe postoperative swelling of resorbable membranes [29] in certain cases could result in unsatisfied patients and dentists. Therefore, a new kind of biodegradable and biocompatible membrane with good mechanical strength must be developed to benefit both patients and dentists.

Recently Mg alloys have been extensively conducted as biodegradable materials. However, rapid corrosion rate, release of hydrogen gas, and lack of long-term mechanical integrity restrict the clinical applications of Mg alloys [30]. Alloying is used to improve the corrosion resistance of Mg alloys and REEs (yttrium, neodymium, and gadolinium [16, 31]) are applied to produce magnesium alloys. Thus, we selected Mg alloys containing REEs, namely, WE43 and Mg3Gd, and a preliminary study was performed to determine whether these alloys can be used as GBR membranes. In this study, all Mg alloys specimens are compact to prevent the ingrowth of soft tissue to the greatest extent in the initial time during degradation period. As Mg alloys degraded, pitting corrosion occurred and a rough surface formed. And we want this rough surface to help cell attachment.

4.1 Sample microstructure and corrosion behavior analysis

It had been reported that yttrium, neodymium and gadolinium can help refine Mg substrate [32, 33]. In this study, the coarse particles and bright intermetallic phases on the surface of two Mg alloys may also be REE-rich precipitates [33] but the grain size of WE43 and Mg3Gd was quite

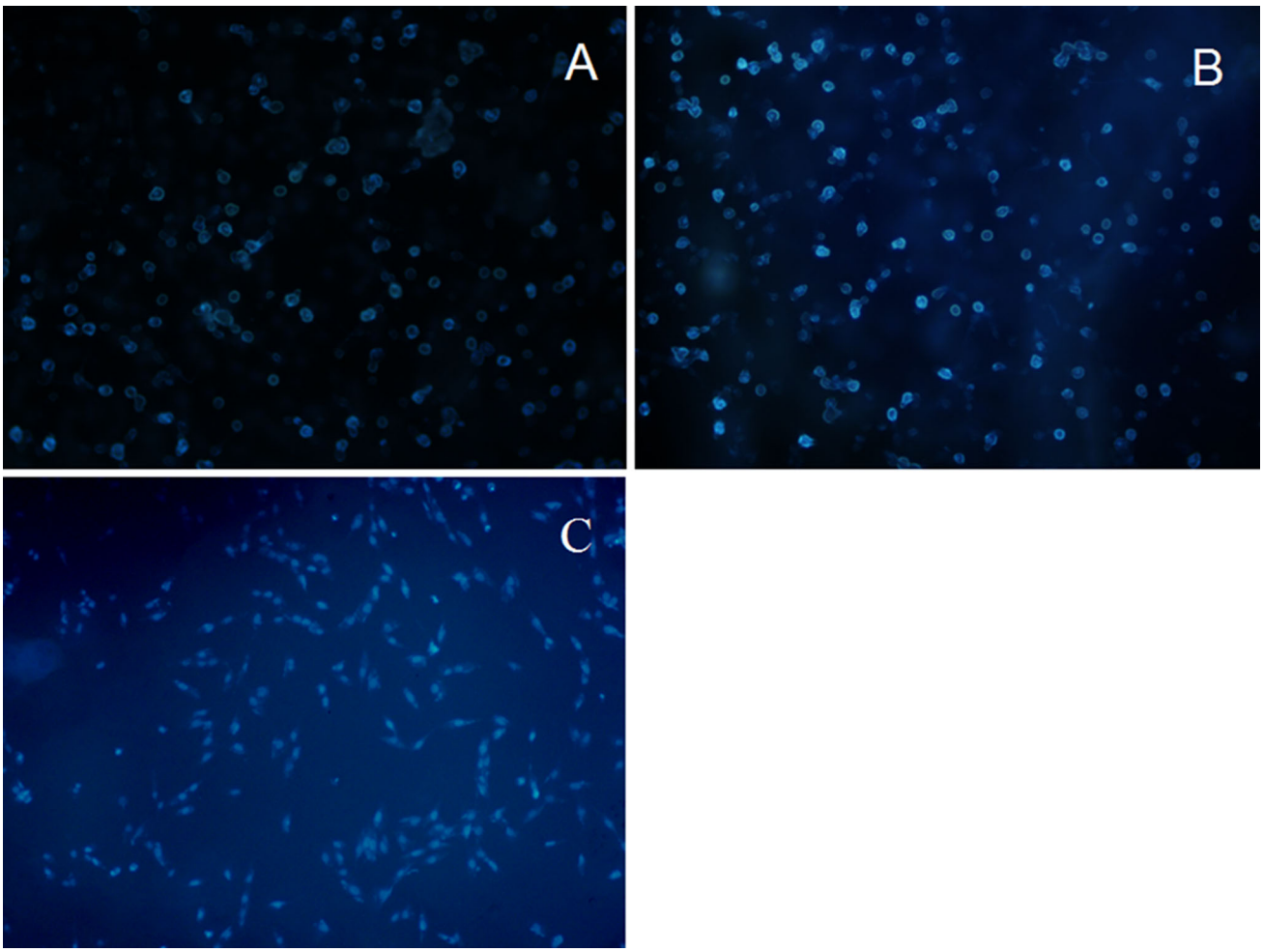

Fig. 9 Adhered MG63 cells after culture on the surface of **a** WE43, **b** Mg3Gd, and **c** Heal-All membranes for 6 h under 400× magnification

different from other researchers [34], it may because our Mg alloys were as-extruded [17]. It seemed that Y and Nd may more efficiently refine the Mg substrate than Gd (Fig. 1a, b) because of the grains size and the number of coarse particles and bright intermetallic phases, but the more refined WE43 did not show better corrosion resistance than Mg3Gd (Fig. 3a). That is, the corrosion behavior of the two Mg alloys was similar in immersion test (Fig. 3). The corrosion products layer can protect the Mg substrate from further degradation [18], thereby decreasing the degradation rate of WE43 and Mg3Gd. Though corrosion rate in vivo may be 1–4 times lower than the corrosion rate in vitro for Mg alloys [35], the two Mg alloys still corroded too fast in this study, especially compared with Heal-All membrane. Therefore, the two Mg alloys should be strongly improved to promote their corrosion resistance.

After immersion for 6 days, large amounts of salt precipitates were deposited and covered the surface of the two Mg alloy, but just a little deposition was seen on the surface of the Heal-All membrane (Fig. 4). The corrosion product of WE43 and Mg3Gd were mainly composed of O, Mg, P, and Ca, and element Y, Nd and Gd were also funded though regardless of their low content. As for Heal-All membrane, the main elements included C and O because the Heal-All membrane consisted of collagen fibers (Fig. 5). Generally, in calcified tissues, such as bones and teeth, calcium phosphate apatite exhibits good osteoconductivity on the surface [26], thus, WE43 and Mg3Gd may facilitate bone formation due to their corrosion product while Heal-All membrane could not.

During their degradation, WE43 and Mg3Gd samples produced an alkaline micro-environment while an acidic micro-environment was formed by Heal-All membrane, which is same as other Mg alloys [18] and resorbable membranes [29]. It is reported that acidic environment is beneficial to osteoclast-induced bone resorption [36] while ALP catalyzes the hydrolysis of phosphate esters to promote mineralization at alkaline pH [27, 36], which indicated that WE43 and Mg3Gd may have better affinity to mineralization than Heal-All membrane.

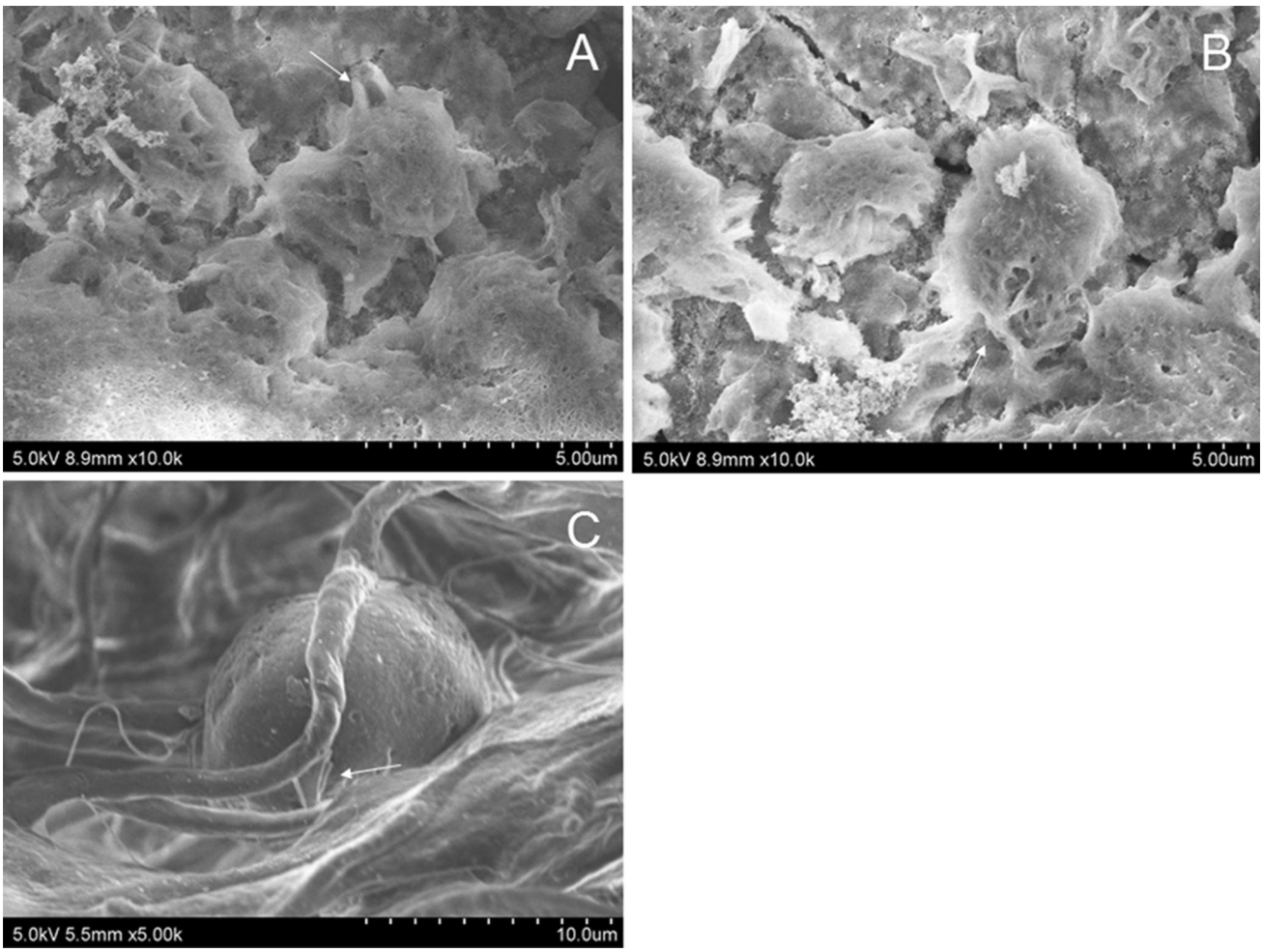

Fig. 10 SEM images of MG63 cells adhered on the surface of **a** WE43, **b** Mg3Gd, and **c** Heal-All membrane; the arrow indicates pseudopods stretched by MG63 cells

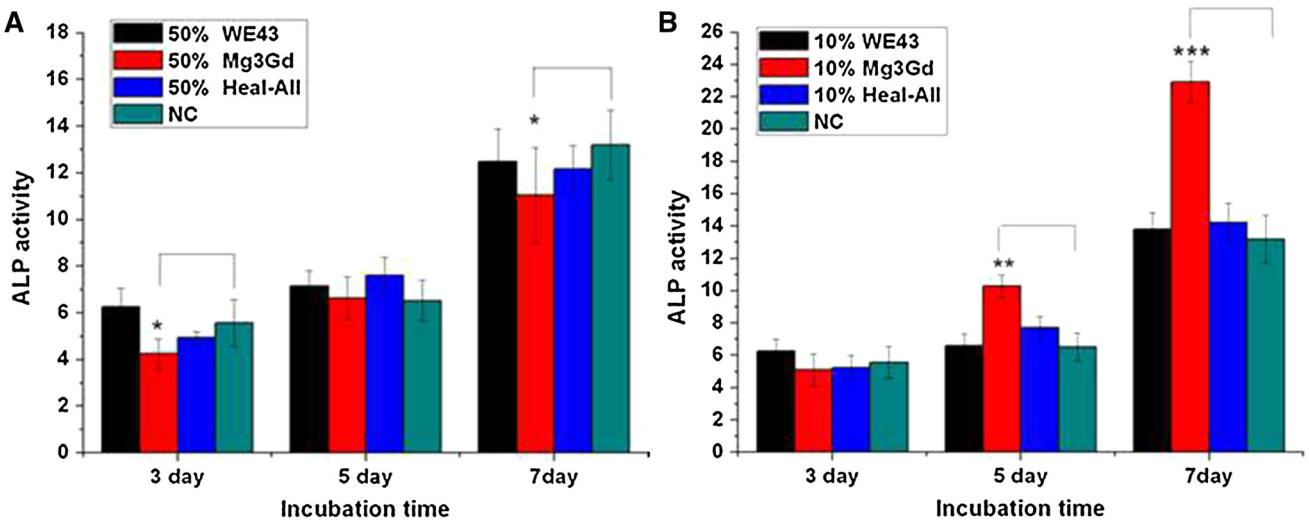

Fig. 11 ALP activity of MG63 cells cultured in **a** 50 % and **b** 10 % extracts for 3, 5, and 7 days (*$P < 0.05$, **$P < 0.01$, ***$P < 0.001$)

After immersion and acid washing, pits and cracks were detected on the surface of the two Mg alloys (Fig. 2a, b) and crack of collagen fibers was seen on Heal-All membrane (Fig. 2c). Despite the pits on two Mg alloys and the crack of collagen fibers on Heal-All membrane, both Mg substrate and collagen matrix remained intact so that Mg alloys and Heal-All membrane could keep their barrier function, indicating that three type of materials fufilled the criteria of cell occlusiveness at day 6. After immersion for 12 days, the collagen matrix was still intact. However, after immersion for 8 days, both two Mg alloys showed porous appearance under naked eyes and they even cracked into pieces at day 12, thus lost their barrier function. Therefore, it is reconfirmed that the corrosion resistance of WE43 and Mg3Gd should be improved from the view of keeping barrier function.

4.2 Biocompatibility analysis

Cytotoxicity and proliferation data showed that 100 % Mg-REE extracts reduced MG63 cell viability. This finding may be due to high pH and osmolality [37] caused by high ion concentration in Mg-REE alloys. However, with the scour and dilution of blood flow, the corrosion product was unable to accumulate to a high extent in the local area in vivo. As such, Mg-REE and Heal-All extracts were diluted. The diluted Mg-REE extracts evidently showed improved cytocompatibility, similar to those reported in a previous study [33]. As predicted, each concentration of the Heal-All extracts did not adversely affect MG63 cell viability (Figs. 6c and 7c). Despite the statistically significant difference among different experimental groups of diluted extracts, the present results indicate that the two Mg-REE alloys satisfied cytocompatibility requirements in vitro for medical applications. The cell adhesion experiment was then conducted to evaluate the in vitro tissue integration of three materials. Figure 9 showed the number of MG63 cells adhered on the three type of materials was almost the same. However, MG63 cells on the Heal-All membrane was surrounded by and adhered to collagen fibers, thus showed the best morphology compared with those on WE43 and Mg3Gd (Fig. 10). It may due to that collagen fibers may act as a reservoir in the cell–matrix attachment of osteogenic cells [38]. Therefore, all materials can support cell attachment but animal study is indispensable to further evaluate the in vivo tissue integration of WE43 and Mg3Gd. Anyway, both WE43 and Mg3Gd showed good in vitro biocompatibility according to cytotoxic, proliferation and adhesion test.

4.3 ALP activity analysis

ALP is an early osteoblastic differentiation marker which was evaluated to determine whether the extracts of the three materials were osteoinductive (Fig. 11). For Mg3Gd, 50 % extract inhibited ALP activity at days 3 and 7, whereas 10 % extract promoted ALP activity at days 5 and 7. This finding may due to the local concentration of Mg^{2+}. Moderate Mg^{2+} concentrations enhance osteogenic activity [39], whereas high Mg^{2+} concentrations inhibit mineralized matrix deposition [40]. However, for WE43, neither 50 nor 10 % extract showed an inhibitory or promotion effect on MG63 ALP activity. Studies showed that in vitro and in vivo corrosion of the same Mg alloy varied because of proteins and other components in body fluids [35, 41]. In the present study, all extracts were prepared in DMEM containing 10 % FBS. Although the degradation tendency was similar between WE43 and Mg3Gd in SBF, the degradation behavior of both alloys may differ in DMEM. Thus, Mg^{2+} concentration in the 50 and 10 % extracts of WE43 may be too low to affect ALP activity. However, the membrane extract showed little effect on early osteogenic activity. Thus, Mg3Gd may help to promote and accelerate bone regeneration if it is improved to be used as GBR membranes, considering its intrinsic effect on the ALP activity of MG63 cells.

5 Conclusion

In this study, two types of Mg-REEs alloys, WE43 and Mg3Gd, were compared with Heal-All membrane. Results showed that both two Mg alloys had good biocompatibility, which made them suitable as medical applications. Moreover, the 10 % extract of Mg3Gd could increase the ALP activity of MG63 cells, which may promote the mineralization [36], accelerate bone regeneration, and shorten the healing time. However, compared with Heal-All membrane, the too-fast degradation of two Mg alloys inhibited them to be used as GBR membrane due to the compromised cell occlusiveness and loss of barrier function. Besides, the in vivo tissue integration and clinical manageability of WE43 and Mg3Gd should also be further determined whether they can fulfill the criteria or not.

Most importantly, the study presented here, which only in its preliminary stages, highlighted the potential of these Mg-REE alloys for uses in bone regeneration. Certainly, further studies and refinements are obviously required. For example, the corrosion resistance of these Mg-REE alloys should be further improved to consistent with the duration of bone regeneration. Besides, Mechanical properties, in vivo corrosion behavior and the promotion of bone regeneration in vivo of either Mg-REE alloys or Heal-All membrane should be evaluated and compared to determine whether Mg-REE alloys could be used as GBR membranes.

Acknowledgments Authors appreciate the Northwest Institute For Non-ferrous Metal Research for providing Mg alloy samples freely.

References

1. Dahlin C, Linde A, Gottlow J, et al. Healing of bone defects by guided tissue regeneration. Plast Reconstr Surg. 1988;81:672–6.
2. Dahlin C, Sennerby L, Lekholm U, et al. Generation of new bone around titanium implants using a membrane technique: an experimental study in rabbits. Int J Oral Maxillofac Implants. 1989;4:19–25.
3. Dahlin C, Gottlow J, Linde A, et al. Healing of maxillary and mandibular bone defects using a membrane technique. An experimental study in monkeys. Scand J Plast Reconstr Surg Hand Surg. 1990;24:13–9.
4. Rakhmatia Yunia Dwi, Ayukawa Yasunori, Furuhashi Akihiro, et al. Current barrier membranes: titanium mesh and other membranes for guided bone regeneration in dental applications. J Prosthodont Res. 2013;57:3–14.
5. Rothamel D, Schwarz F, Fienitz T, et al. Biocompatibility and biodegradation of a native porcine pericardium membrane: results of in vitro and in vivo examinations. Int J Oral Maxillofac Implants. 2012;27:146–54.
6. Ronda M, Rebaudi A, Torelli L, et al. Expanded vs. dense polytetrafluoroethylene membranes in vertical ridge augmentation around dental implants: a prospective randomized controlled clinical trial. Clin Oral Implants Res. 2014;25:859–66.
7. Hammerle CH, Jung RE. Bone augmentation by means of barrier membranes. Periodontology. 2000;33:36–53.
8. Zhang J, Xu Q, Huang C, et al. Biological properties of an antibacterial membrane for guided bone regeneration: an experimental study in rats. Clin Oral Implants Res. 2010;21:321–7.
9. McGinnis M, Larsen P, Miloro M, Beck M. Comparison of resorbable and nonresorbable guided bone regeneration materials: a preliminary study. Int J Oral Maxillofac Implants. 1998;13:30–5.
10. Wang HX, Guan SK, Wang YS, et al. In vivo degradation behavior of Ca-deficient hydroxyapatite coated Mg–Zn–Ca alloy for bone implant application. Colloids Surf B. 2011;88(1):254–9.
11. Witte F. The history of biodegradable magnesium implants: a review. Acta Biomater. 2010;6:1680–92.
12. Revell PA, Damien E, Zhang XS, et al. The effect of magnesium ions on bone bonding to hydroxyapatite. Key Eng Mater. 2004;254–256:447–450.
13. Witte F, Kaese V, Haferkamp H, et al. In vivo corrosion of four magnesium alloys and the associated bone response. Biomaterials. 2005;26:3557–63.
14. Alvarez-Lopez M, Pereda MD, del Valle JA, et al. Corrosion behaviour of AZ31 magnesium alloy with different grain sizes in simulated biological fluids. Acta Biomater. 2010;6:1763–71.
15. Zhao Nan, Workman Benjamin, Zhu Donghui. Endothelialization of novel magnesium-rare earth alloys with fluoride and collagen coating. Int J Mol Sci. 2014;15:5263–76.
16. Hort N, Huang Y, Fechner D, et al. Magnesium alloys as implant materials—principles of property design for Mg-RE alloys. Acta Biomater. 2010;6:1714–25.
17. Gong H, Wang K, Strich R, et al. In vitro biodegradation behavior, mechanical properties, and cytotoxicity of biodegradable Zn–Mg alloy. J Biomed Mater Res B. 2015;103:1632–40.
18. Johnson I, Perchy D, Liu H. In vitro evaluation of the surface effects on magnesium–yttrium alloy degradation and mesenchymal stem cell adhesion. J Biomed Mater Res A. 2012;100:477–85.
19. Liu W, Cao F, Chang L, et al. Effect of rare earth element Ce and La on corrosion behavior of AM60 magnesium alloy. Corros Sci. 2009;51:1334–43.
20. Di Mario C, Griffiths H, Goktekin O, et al. Drug-eluting bioabsorbable magnesium stent. J Interv Cardiol. 2004;17:391–5.
21. Agrawal CM, Mani G, Feldman MD, et al. Coronary stents: a materials perspective. Biomaterials. 2007;28:1689–710.
22. Arrabal R, Matykina E, Pardo A, et al. Corrosion behaviour of AZ91D and AM50 magnesium alloys with Nd and Gd additions in humid environments. Corros Sci. 2012;55:351–62.
23. Kokubo T, Takadama H. How useful is SBF in predicting in vivo bone bioactivity? Biomaterials. 2006;27:2907–15.
24. Liu L, Li N, Lei T, et al. The in vitro biological properties of Mg–Zn–Sr alloy and superiority for preparation of biodegradable intestinal anastomosis rings. Med Sci Monit. 2014;20:1056–66.
25. Gu XN, Zhou WR, Zheng YF, et al. Corrosion fatigue behaviors of two biomedical Mg alloys—AZ91D and WE43—in simulated body fluid. Acta Biomater. 2010;6:4605–13.
26. Pan YK, Chen CZ, Wang DG, et al. Effects of phosphates on microstructure and bioactivity of micro-arc oxidized calcium phosphate coatings on Mg–Zn–Zr magnesium alloy. Colloids Surf B. 2013;109:1–9.
27. Kunjukunju S, Roy A, Ramanathan M, et al. A layer-by-layer approach to natural polymer-derived bioactive coatings on magnesium alloys. Acta Biomater. 2013;9:8690–703.
28. Scantlebury TV. 1982–1992: a decade of technology development for guided tissue regeneration. J Periodontol. 1993;64:1129–37.
29. van Leeuwen AC, Huddleston Slater JJR, Gielkens PFM, et al. Guided bone regeneration in rat mandibular defects using resorbable poly(trimethylene carbonate) barrier membranes. Acta Biomater. 2012;8:1422–9.
30. Chai H, Guo L, Wang X, et al. In vitro and in vivo evaluations on osteogenesis and biodegradability of a β-tricalcium phosphate coated magnesium alloy. J Biomed Mater Res A. 2012;100:293–304.
31. Li M, Cheng Y, Zheng YF, et al. Surface characteristics and corrosion behaviour of WE43 magnesium alloy coated by SiC film. Appl Surf Sci. 2012;258:3074–81.
32. Gao L, Chen RS, Han EH. Effects of rare-earth elements Gd and Y on the solid solution strengthening of Mg alloys. J Alloys Compd. 2009;481:379–84.
33. Willbold E, Gu X, Albert D, et al. Effect of the addition of low rare earth elements (lanthanum, neodymium, cerium) on the biodegradation and biocompatibility of magnesium. Acta Biomater. 2015;11:554–62.
34. Brar HS, Berglund IS, Allen JB, et al. The role of surface oxidation on the degradation behavior of biodegradable Mg-RE (Gd, Y, Sc) alloys for resorbable implants. Mater Sci Eng C. 2014;40:407–17.
35. Martinez Sanchez AH, Luthringer BJC, Feyerabend F, et al. Mg and Mg alloys: how comparable are in vitro and in vivo corrosion rates? A review. Acta Biomater. 2015;13:16–31.
36. Clarke B. Normal bone anatomy and physiology. Clin J Am Soc Nephrol. 2008;3:S131–9.
37. Fischer J, Prosenc MH, Wolff M, et al. Interference of magnesium corrosion with tetrazolium-based cytotoxicity assays. Acta Biomater. 2010;6:1813–23.
38. Taguchi Y, Amizuka N, Nakadate M, et al. A histological evaluation for guided bone regeneration induced by a collagenous membrane. Biomaterials. 2005;26:6158–66.
39. Yoshizawa S, Brown A, Barchowsky A, et al. Magnesium ion stimulation of bone marrow stromal cells enhances osteogenic activity, simulating the effect of magnesium alloy degradation. Acta Biomater. 2014;10(6):2834–42.
40. Zhang Li, Yang Chunxi, Li Jiao, et al. High extracellular magnesium inhibits mineralized matrix deposition and modulates intracellular calcium signaling in human bone marrow-derived mesenchymal stem cells. Biochem Biophys Res Commun. 2014;450:1390–5.
41. Scheideler L, Füger C, Schille C, et al. Comparison of different in vitro tests for biocompatibility screening of Mg alloys. Acta Biomater. 2013;9:8740–5.